Oral Presentation

The 7th TSME International Conference on Mechanical Engineering
13-16 December 2016

AMM0008

An Energy Method for Analysis of Belleville Springs

Watcharapong Patangtalo[1*], Sontipee Aimmanee[1], and Surachate Chutima[2]

[1] Advanced Materials and Structures Laboratory: AMASS, Mechanical Engineering Department,
King Mongkut's University of Technology Thonburi, 126 Pracha Uthit Rd, Bang Mot, Thung Khru, Bangkok, 10140, Thailand
[2] Centre of Operation for Computer Aided Research Engineering: COCARE, Mechanical Engineering Department,
King Mongkut's University of Technology Thonburi, 126 Pracha Uthit Rd, Bang Mot, Thung Khru, Bangkok, 10140, Thailand
[*] Corresponding Author: E-mail wp.me44@gmail.com, Telephone Number +66-84-016-0545

Abstract

This topic discusses an improved methodology for solving the deformation behavior of a Belleville spring under axial loading by the minimum potential energy principle. The elastic strain energy and work done of the Belleville spring are formulated based on the classical thin shell theory in a conical coordinate system. The von Karman and Reissner approximations to the nonlinear strain-displacement relations take the geometrical effects of the moderately and very large axial deflection into consideration, respectively. The Ritz method is used to solve for the deformation and force characteristics of isotropic springs and the solutions are compared with the previous Almen and Laszlo's equation, experiments and the finite element analysis. The present energy model can capture the effect of a geometric parameter that has been missing from the Almen and Laszlo scheme. The comparison exhibits that the developed method gives very good agreement with the results from the testing and finite-element method, whereas Almen and Laszlo's equation overpredicts the applied load at a given deflection in most cases owing to their limited assumptions.

Keywords: Belleville Spring, Energy Method, Geometrical Nonlinearities, Snap-through

1. Introduction

A Belleville spring or coned-disc spring as shown in Fig.1 is a type of spring shaped like a washer. It can be loaded along its axis and deformed elastically similar to other type of springs. Particularly, a Belleville spring is suitable for axial loading with either linear or nonlinear spring characteristic. It is also applicable in applications that need the buckling of spring as illustrated in Fig. 2. The overall relationship between compressive axial load P and the corresponding deflection δ in the figure is shown as a function of the ratio of height to thickness (h/t). According to Almen and Laszlo [1], the relationship between the load and deflection is illustrated to be linear, if the ratio of h/t is quite less than the square root of two. If the ratio of h/t is equal to or higher than the square root of two, the relationship is not linear and can reveal negative spring stiffness or negative spring rate. When the load increases and reaches the upper critical point right before the negative rate region, the spring is suddenly snapped into the inverted shape on the ensuing positive rate region where suddenly large axial deflection is observed. On the contrary, when the applied load descends from the snapped configuration to the lower critical point, the spring is snapped back close to the original undeformed shape. The abrupt shape-change phenomenon is called "oil canning" or "snap-through buckling" and happens because the spring is statically unstable in the negative rate region.

A Belleville spring is basically a truncated conical shell. Previous research of stability of this type of structure was originally conducted by Pflüger [2]. Later, many researchers have investigated instability and buckling of isotropic conical shells caused by a variety of applied loads. Seide [3, 4] examined the buckling effect of conical shells on axial load. Together with Weigarden and Morgan [5, 6], they studied the stability of conical shell under axial compression and other external forces. Singer [7] proposed the solution for the buckling of conical shells under external force. With Baruch [8] they considered the buckling of stiffened conical shells under the static hydraulic pressure. Moreover, Singer, Baruch and Harari [9, 10] also analyzed the buckling of the conical shell and found buckling phenomena caused by the axially compression with different conditions.

All of the investigations mentioned above considered thin shell with high cone angle over 45 degree. (β in Fig. 1) but did not study the behavior of shells that has low and moderate cone angle as presented in the Belleville spring shapes. Some researchers, therefore, created a mathematical model for analyzing the Belleville spring using the specific kinematics assumptions to predict the behavior of the Belleville spring. For example, Almen and Laszlo [1] presented a mathematical formulation that shows relationship among axial load, deflection, and stresses developed in a Belleville spring made of isotropic material. Their assumptions and equations were based on the method of Timoshenko [11], which assumes that the cross-sectional area is undestroyed; deflection is caused only by the rotation of cross sectional area around the neutral point, and the radial stress is equal to zero. Curti and Orlando [12, 13] modified the assumptions of Almen and Laszlo and set the radial

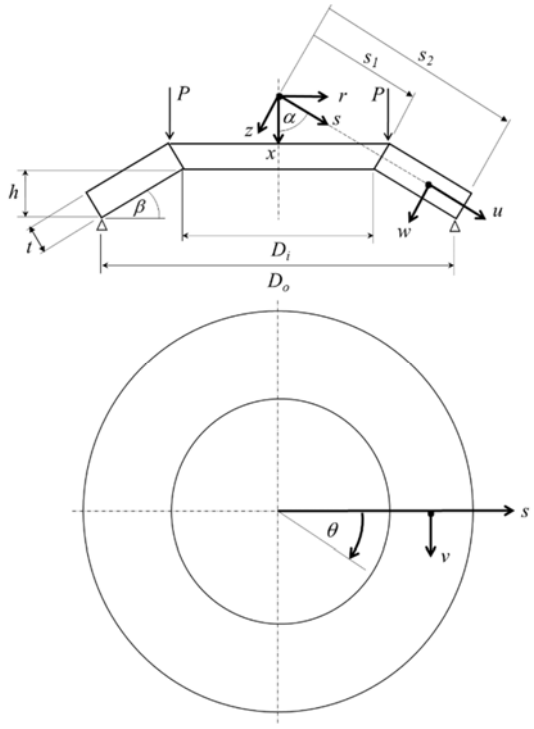

Fig. 1 Belleville spring geometry and coordinate system used

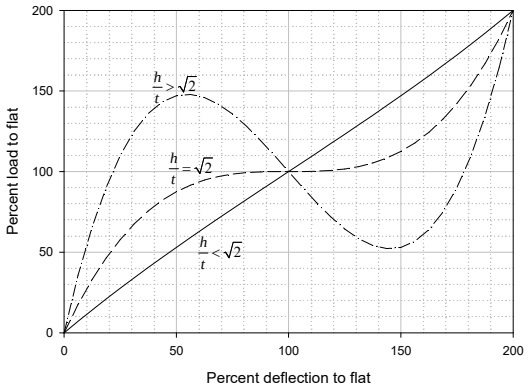

Fig. 2 Load-deflection characteristics

to zero instead of stress. Zheng et al. [14] also formulated a cone disk spring design equation for isotropic springs. They developed an analytical model by treating a spring as a circular plane plate with initial bending curvature. The energy method was proposed for calculating the relationship of load and deflection. Ozaki and Tsuda [15] investigated the effects of friction boundary condition on the static and dynamic deformation behaviors of stacked Belleville springs by using FEM. In addition, with the improvement of testing and numerical method in recent years, new techniques for preventing material failure of steel Belleville spring parts were proposed [16-17].

To relax the assumptions stated above, this article presents the new formulation for analysis of the Belleville spring made from isotropic materials. The study is directly related to the relevant parameters such as size, shape and material of spring based on the theory of thin structures, which is concerned large deflection and the buckling instability caused by geometric nonlinearities. The structure of the article is arranged as follows; energy method based on the Ritz approach is elaborated in the next section. Parametric study of Belleville spring's characteristics is conducted in Section 3. Comparison of load-displacement relationships of various spring geometries calculated from Almen and Laszlo's equation, experiments, the present energy method, and the finite-element method are investigated. The final conclusion is given in Section 4.

2. Modeling of Belleville Spring

Due to the limitation from Almen and Laszlo's assumptions, this section aims to create the generic formulation developed by using the energy principle.

2.1 Strain-displacement and stress-strain relations

Starting from the expressions of strain and displacement of a conical shell generated under the Kirchhoff-Love hypothesis and Donnell shallow shell approximation, the assumptions are as followed: (1) the spring is adequately thin, and (2) strains are sufficiently small. This two conditions are typically valid for general Belleville springs in application. All of the assumptions in the Almen and Laszlo model outlined in Introduction are released in this work.

Accordingly, the strains are given by

$$\begin{aligned} \varepsilon_s &= \varepsilon_s^o + z\kappa_s^o \\ \varepsilon_\theta &= \varepsilon_\theta^o + z\kappa_\theta^o \\ \gamma_{s\theta} &= \gamma_{s\theta}^o + z\kappa_{s\theta}^o \end{aligned} \tag{1}$$

The quantities ε_s^o, ε_θ^o, $\gamma_{s\theta}^o$ and κ_s^o, κ_θ^o, $\kappa_{s\theta}^o$ are the mid-plane strains and curvatures, respectively. The relationship between strains and mid-plane displacements can be expressed as:

$$\begin{aligned} \varepsilon_s^o &= \frac{\partial u^o}{\partial s} + \underline{\frac{1}{2}\left(\frac{\partial w^o}{\partial s}\right)^2} \\ \varepsilon_\theta^o &= \frac{u^o - w^o\cot\alpha}{s} + \frac{1}{s\sin\alpha}\frac{\partial v^o}{\partial\theta} + \underline{\frac{1}{2}\left(\frac{1}{s\sin\alpha}\frac{\partial w^o}{\partial\theta}\right)^2} \\ \gamma_{s\theta}^o &= \frac{\partial v^o}{\partial s} - \frac{v^o}{s} + \frac{1}{s\sin\alpha}\frac{\partial u^o}{\partial\theta} + \underline{\frac{1}{s\sin\alpha}\frac{\partial w^o}{\partial s}\frac{\partial w^o}{\partial\theta}} \\ \kappa_s^o &= -\frac{\partial^2 w^o}{\partial s^2} \\ \kappa_\theta^o &= -\frac{1}{s}\frac{\partial w^o}{\partial s} - \frac{1}{s^2\sin^2\alpha}\frac{\partial^2 w^o}{\partial\theta^2} \\ \kappa_{s\theta}^o &= -\frac{2}{\sin\alpha}\frac{\partial}{\partial s}\left(\frac{1}{s}\frac{\partial w^o}{\partial\theta}\right) \end{aligned} \tag{2}$$

when u^o, v^o and w^o are the mid-plane displacements in conical coordinate system (s-θ-z coordinate) as

illustrated in Fig. 1. The conical coordinate system used in this work simply relates to the cylindrical coordinate by the coordinate rotation between *s*-*z* axes and *r*-*x* axes with the cone angle β ($\beta = 90^{o}-\alpha$) as shown in the figure so the strains and displacements in the conical coordinate can be derived by tensor transformation from the cylindrical coordinate. It must be noted that the underlined terms in Equation (2) explicitly represent the von Karman approximation to full nonlinear strain-displacement relations in order to capture moderately large axial deflection of the spring. On the contrary, Almen and Laszlo implicitly took the nonlinear strain-displacement relations into account when kinematics of a conical disk spring was formulated. With the assumption of small deflection angle from angle β, they expressed strain as a second order polynomial of the axial deflection.

The constitutive stress-strain relations for a given layer is

$$\begin{aligned}\sigma_s &= \frac{E}{1-\nu^2}\varepsilon_s + \frac{\nu E}{1-\nu^2}\varepsilon_\theta \\ \sigma_\theta &= \frac{\nu E}{1-\nu^2}\varepsilon_s + \frac{E}{1-\nu^2}\varepsilon_\theta \\ \tau_{s\theta} &= G\gamma_{s\theta}\end{aligned} \tag{3}$$

where σ_s ,σ_θ and $\tau_{s\theta}$ are normal stresses in the *s*- and θ- directions and in-plane shear stress in the *s*-θ plane, respectively. *E* is extensional modulus, *v* Poisson's ratio and *G* the shear modulus.

2.2 Classical lamination theory

The relationship between force and moment resultants and the mid-plane strains-curvatures is calculated from *ABD* matrix and can be described as: [18]

$$\begin{Bmatrix} N_s \\ N_\theta \\ N_{s\theta} \\ M_s \\ M_\theta \\ M_{s\theta} \end{Bmatrix} = \begin{bmatrix} A_{11} & A_{12} & A_{16} & B_{11} & B_{12} & B_{16} \\ A_{12} & A_{22} & A_{26} & B_{12} & B_{22} & B_{26} \\ A_{16} & A_{26} & A_{66} & B_{16} & B_{26} & B_{66} \\ B_{11} & B_{12} & B_{16} & D_{11} & D_{12} & D_{16} \\ B_{12} & B_{22} & B_{26} & D_{12} & D_{22} & D_{26} \\ B_{16} & B_{26} & B_{66} & D_{16} & D_{26} & D_{66} \end{bmatrix} \begin{Bmatrix} \varepsilon_s^o \\ \varepsilon_\theta^o \\ \gamma_{s\theta}^o \\ \kappa_s^o \\ \kappa_\theta^o \\ \kappa_{s\theta}^o \end{Bmatrix} \tag{4}$$

Force and moment resultants in Equation (4) are associated with the relevant stress component from the following equations

$$\begin{aligned}\{N_s, N_\theta, N_{s\theta}\} &= \int_{z_0}^{z_n} \{\sigma_s, \sigma_\theta, \tau_{s\theta}\} dz \\ \{M_s, M_\theta, M_{s\theta}\} &= \int_{z_0}^{z_n} \{\sigma_s, \sigma_\theta, \tau_{s\theta}\} z dz\end{aligned} \tag{5}$$

where σ_s ,σ_θ and $\tau_{s\theta}$ are normal stresses in the *s*- and θ- directions and in-plane shear stress in the *s*-θ plane. A_{ij}, B_{ij} and D_{ij} in *ABD* matrix can be calculated from Equation (6)

$$[A] = \begin{bmatrix} \frac{E}{1-\nu^2} & \frac{\nu E}{1-\nu^2} & 0 \\ \frac{\nu E}{1-\nu^2} & \frac{E}{1-\nu^2} & 0 \\ 0 & 0 & G \end{bmatrix} t$$

$$[B] = 0 \tag{6}$$

$$[D] = \begin{bmatrix} \frac{E}{1-\nu^2} & \frac{\nu E}{1-\nu^2} & 0 \\ \frac{\nu E}{1-\nu^2} & \frac{E}{1-\nu^2} & 0 \\ 0 & 0 & G \end{bmatrix} \frac{t^3}{12}$$

2.3 The Ritz method

Under the axial loading mid-plane displacements of the Belleville spring in the radial direction *u*, circumferential direction *v*, and transverse direction *w* in the conical coordinate system illustrated in Fig.1 are assumed to be

$$\begin{aligned} u^o &= \sum_{i=0}^{I} a_i s^i \\ v^o &= 0 \\ w^o &= \sum_{k=0}^{K} c_k s^k \end{aligned} \tag{7}$$

Because the axisymmetric deformation of the Belleville spring is considered, circumferential displacement *v* must be zero, whereas the displacements in the other two directions are expressed as polynomial functions only in the *s*-direction. a_i, b_j and c_k are unknown coefficients, which are determined by utilizing the minimum total potential energy principle in conjunction with the Ritz method. *I* and *K* indicate the maximum order of polynomials for the displacements in *s*- and *z*-directions, respectively.

The total potential energy of the Belleville spring Π in Equation (8) can be formulated as the combination of the strain energy *U* expressed in Equation (9), the external work done *W* exerted by axial force *P* in Equation (10) and the constraint term *g* in Equation (11)

$$\Pi = U - W - \lambda g \tag{8}$$

AMM0008

$$U = \frac{1}{2}\int_0^{2\pi}\int_{s_1}^{s_2}(N_s\varepsilon_s^o + N_\theta\varepsilon_\theta^o + N_{s\theta}\gamma_{s\theta}^o + M_s\kappa_s^o + M_\theta\kappa_\theta^o + 2M_{s\theta}\kappa_{s\theta}^o)s\sin\alpha\, ds\, d\theta \quad (9)$$

$$W = u(s_p)P\cos\alpha + w(s_p)P\sin\alpha \quad (10)$$

$$g = u(s_2)\cos\alpha + w(s_2)\sin\alpha \quad (11)$$

In the above, s_1 and s_2 in Equations (9) and (11) are the inner and outer radial distances from the vertex of the cone shown in Fig.1, while s_p in Equation (10) denotes the radial distance where the load P is exerted. If application of P is distributed on the top of the spring, s_p is equal to s_1. The constraint in Equation (11) is required to ensure that the bottom edge of spring ($s = s_2$) is immovable in the vertical direction ($g = 0$) but it can slide in the horizontal direction. λ is Lagrange multiplier associated with the constraint function g. It is important to note that the formulation developed herein is based on material or Lagrangian description in which displacements, strains and stresses are functions of the reference or undeformed coordinate (s-θ-z) located on the undeformed spring mid-surface. Therefore, the coordinate angle α relative to the vertical (as well as original cone angle β) is invariant during the spring deformation because it is referred to the original spring shape.

To warrant equilibrium of the spring's deformation under the exerted load P, the first variation of Equation (8) must be equal to zero. As a result, the unknown a_i and c_k can be obtained from the following nonlinear system of equations

$$\begin{aligned}\frac{\partial}{\partial a_i}(U - W) - \lambda\frac{\partial g}{\partial a_i} &= 0\\ \frac{\partial}{\partial c_k}(U - W) - \lambda\frac{\partial g}{\partial c_k} &= 0\\ g &= 0\end{aligned} \quad (12)$$

The unknown coefficients are obtained after solving the system of equations (12) under a given axial load. They are back-substituted into the displacement functions in Equation (7) to calculate for the displacement in any directions. These calculations are performed by using the computational software program Mathematica™. Strain and stress in each direction can also be evaluated by utilizing Equations (2) and (3).

Table 1 Material Properties

Material	E (GPa)	G (GPa)	ν
Steel	206.9	79.6	0.30

3. Results and Discussions

3.1 Load - deflection analysis

For the sake of convenience and brevity, all variables shown in this section are converted into dimensionless quantities. This methodology can reduce the number of independent variables used in the analysis of the obtained results. The variables that affect the load (P) at any deflection of a spring are related to the material properties such as Young Modulus (E), Poisson's ratio (ν), and the geometries of the spring including the height (h), thickness (t), inner diameter (D_i) and outer diameter (D_o) as shown in Figure 2. The Buckingham-Pi theorem is used to normalize these variables. It is found that normalized load P_{nor} depends on three groups of dimensionless variables as shown in Equation (13).

$$P_{nor} = \frac{P\cdot D_o^{\,2}}{E\cdot t^4} = f\left(\frac{D_i}{D_o}, \frac{h}{t}, \frac{h}{D_o}\right) \quad (13)$$

In addition, normalized deflection δ_{nor} can be defined in Equations (14) as the ratio of the topmost deflection to thickness of the spring

$$\delta_{nor} = \frac{\delta}{t} \quad (14)$$

and normalized stress, expressed as the ratio of the circumferential stress to the load per the outer diameter multiplying by thickness, is expressed in Equation (15)

$$\sigma_{nor} = \frac{\sigma_\theta}{P/(D_o\cdot t)} \quad (15)$$

The springs considered for the analysis in subsection 3.2 to 3.3 is made of isotropic steel, of which material properties are tabulated in Table 1. Fig. 3 shows the relationship between normalized load and normalized deflection of a spring with zero cone angle (β) or a flat spring with $h/t = 0$. The figure presents the results from the present energy method, the Almen and Laszlo equation, and the Almen and Laszlo testing. Legend U5W2 indicates that displacement functions $\bar{U}$ and $\bar{W}$ of equation (9) utilized in the energy method are quintic (I = 5) and quadratic (K = 2) polynomials, respectively. The numbers of terms in the polynomials are specified by monitoring convergence of the calculated displacements and strains. NLW denotes the inclusion of geometrically non-linear terms of w, which is underlined in Equation (2). As seen, the result from U5W2-NLW shows non-constant increasing positive spring rate when the applied load is higher. This computation agrees very well with the testing result and exhibits a better prediction than that obtained from the Almen and Laszlo equation, which clearly is an overestimate. Calculation from the energy model

without geometric nonlinearities contribution denoted as merely U5W2 is also plotted in the figure for comparison and it undoubtedly reveals a linear load-displacement relation, which unsatisfactorily underestimates the spring rate at higher deflections.

Fig. 4 displays the results from the spring with h/t = 0.65, which is less than the square root of two. Thus, it is expected that the deformation behavior of spring has only positive spring rate. Analysis with U5W2-NLW again shows a good agreement with the experiment. Results from both the energy method and testing are slightly lower than that obtained from the Almen and Laszlo equation, similar to that illustrated in the previous figure. In addition, the recent formulation developed by Zheng, et al. [14] is also computed and included in Fig. 4. It presents very close prediction to the Almen and Laszlo's formulation. The energy model U5W2 again provides a linear relation with a uniform spring rate, which is mostly overestimated in the range of normalized deflection considered. Henceforth analyses with the present energy model will always take nonlinear kinematics of strain-displacement into account to be able to accurately capture stiffening or softening effect of Belleville springs.

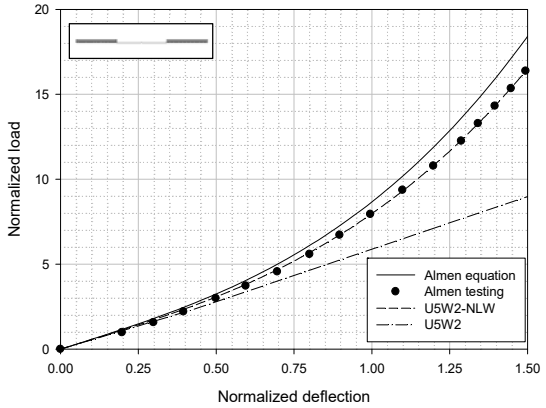

Fig. 3 Load-deflection curve of a flat Belleville spring (D_i/D_o = 0.38, h/D_o = 0, h/t = 0, t/L = 0.064, β = 0°)

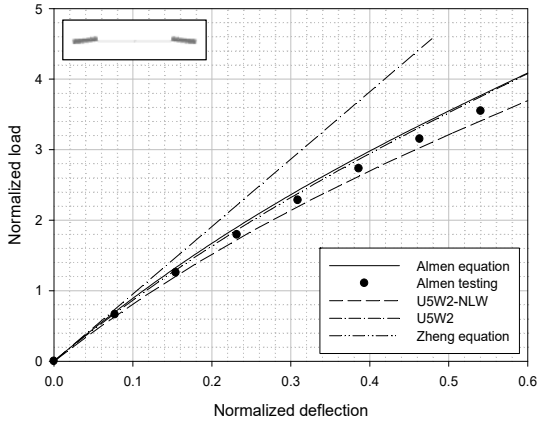

Fig. 4 Load-deflection curve of a Belleville spring having a positive rate only

(D_i/D_o = 0.60, h/D_o = 0.0216, h/t = 0.65, t/L = 0.1648, β = 6.16°)

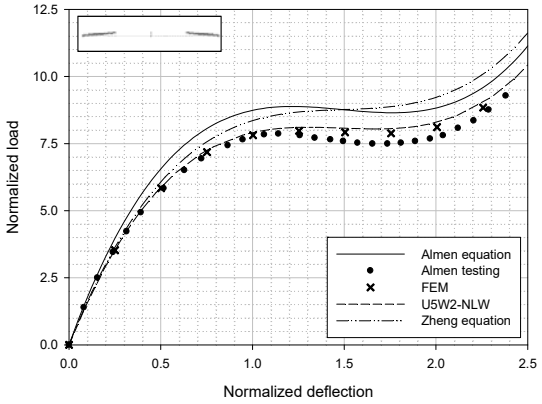

Fig. 5 Load-deflection curve of a Belleville spring having a negative rate (D_i/D_o = 0.51, h/D_o = 0.0208, h/t =1.49, t/L = 0.0569, β = 4.86°)

The spring with h/t more than the square root of two is shown in Fig. 5. The result of relationship between load and deflection from the present energy method shows two points of zero spring rate, i.e. the upper critical point at δ_{nor} approximately equal to 1.2 and lower critical point at δ_{nor} about 1.7. The normalized deflection between the upper and lower critical points reveals negative spring rate, which theoretically indicates unstable deformation. Therefore, when the load increases to the upper critical point, the spring snaps into the new position at δ_{nor} equal to 2.0. On the contrary, when decreasing force reaches lower critical point, the spring snaps back to the normalized deflection of around 1.0. The result from the Almen and Laszlo equation again predicts higher normalized load than those from the energy method and testing results. The model of Zheng, et al. gives the same spring rate as the energy method and testing at small deflections but noticeably overestimates the normalized load when the normalized deflection is larger. Analysis with finite element method (FEM) is also conducted by using commercial software ABAQUS™. Two dimensional axisymmetric elements are chosen for calculation. Simulation output obtained from ABAQUS™ is close to that of the energy method and testing data and absolutely confirms the validity of the present energy model. Thus, the present energy model will be confidently used with ease in parametric studies and performance analyses of Belleville springs in different cases and conditions, since it consumes less preprocessing and computation times than FEM.

Fig. 6 shows examples of the analysis of a spring when load acts away from the edge of inner diameter. D_f denotes diameter of the circular lined load. The spring considered has D_f/D_o ratio of 0.45. Therefore, when the lined load is located at the inner edge of the spring, D_f/D_o ratio equals 0.45. From the figure, the spring with load applying further away from the inner

diameter (larger D_i/D_o) requires higher resultant force for the same deflection. The results of the present energy model are in much better agreement with the Almen and Laszlo experiment than the result predicted by the Almen and Laszlo equation. Simulation from FEM once again matches nicely with the energy model.

Fig. 7 illustrates the mid-plane deformation of the spring along the radial distance at three different topmost deflections (δ = 1, 3, and 6 mm) based on three different methods, namely the present energy model, the Almen and Laszlo model, and FEM. The spring considered in the figure has the upper and lower critical points at the deflections equal to 1.6 and 5 mm, respectively. The spring's deflection of 1 mm shows the identical deformed shape of the mid-plane along the generator line in all three approaches. The spring's mid-plane remains straight line and obeys the Almen and Laszlo's assumption of undestroyed rotational cross-section during this loading. However, as the spring has the deflection of 3 mm, which is beyond the upper critical point, spring exhibits the radially curved deformation according to the present energy method and FEM. This curved cross-section refutes the Almen and Laszlo assumption to a certain extent. At the deflection higher than the lower critical point at 6 mm, the mid-plane deformation shows further noticeable curvature in the radial direction, and therefore the assumption of the Almen and Laszlo equation is further invalid in this case.

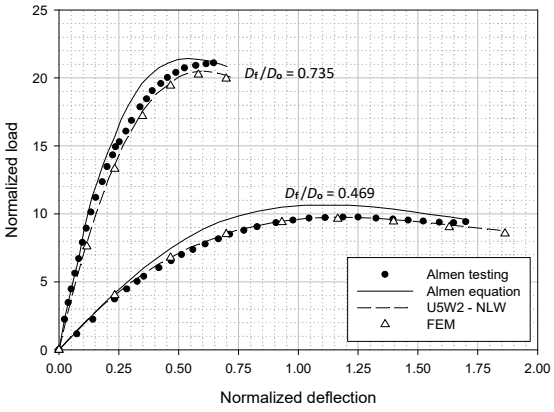

Fig. 6 Load-deflection curve of a Belleville spring loaded at various locations
(D_i/D_o = 0.45, h/D_o = 0.0238, h/t = 1.72, t/L = 0.0508, β = 5.02°)

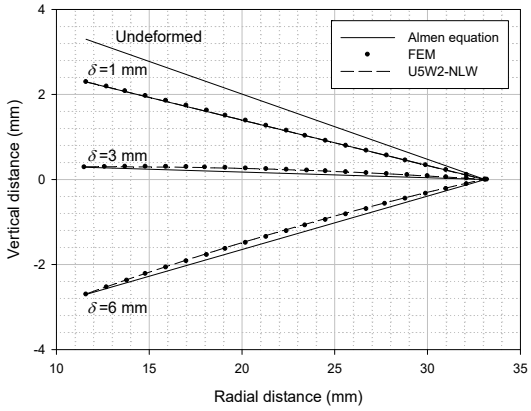

Fig. 7 Deflection of Belleville spring along the radial distance
(D_i/D_o =0.35, h/D_o = 0.05, h/t = 3.3, t/L = 0.0461, β = 8.75°)

3.2 Stress and strain analysis

For analysis and design of a disk spring, circumferential stress is normally considered because of its higher magnitude than stress in the other directions. In this article the circumferential stress is presented in the form of the normalized variable expressed in Equation (15). Fig. 8 and 9 illustrate the stresses for the spring having the same geometric parameters as those used in Fig. 5.

Fig. 8 shows the relations between the normalized load and normalized circumferential stress calculated from the energy method at three transverse locations on the inner edge: top, middle and bottom. The increase of the applied load causes the higher circumferential stress. A compressive stress occurs at the top, while a tensile stress appears at the bottom, as expected in a typical bending structure subjected to a transverse load. It can be noted that because nonlinear effects, the induced stress is not linearly proportional to the applied force.
Fig. 9 shows the circumferential stress along the generator in the *s*-direction when the spring is loaded such that the deflection is equal to the height of spring. At the inner edge ($s = s_1$) the magnitude of compressive stress is highest at the top surface where the force is applied. On the other hand, at the outer edge ($s = s_2$) the maximum tensile stress locates at the bottom surface, where the spring is constrained or supported.

Table 2 Example of maximum stress and strain in circumferential and radial directions

D_i/D_o	h/t	h/D_o	σ_s (MPa)	σ_θ (MPa)	ε_s (μm/m)	ε_θ (μm/m)	% $\lvert\sigma_s/\sigma_\theta\rvert$	% $\lvert\varepsilon_s/\varepsilon_\theta\rvert$
0.35	1.5	0.01	-2.08	-17.96	15	- 83	11.58	17.69
		0.05	-53.43	-452.83	365	-2101	11.80	17.38
	3.3	0.01	-1.40	-8.38	8	-39	16.71	19.18
		0.05	-35.65	-209.98	184	-979	16.98	18.84

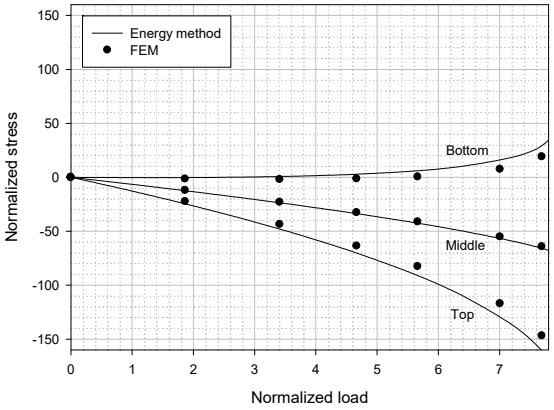

Fig. 8 Stress-load relationship at inner diameter of Belleville spring

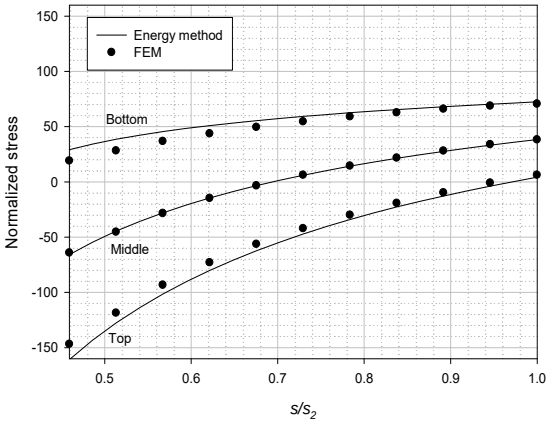

Fig. 9 Stress distribution along the radial direction of Belleville spring

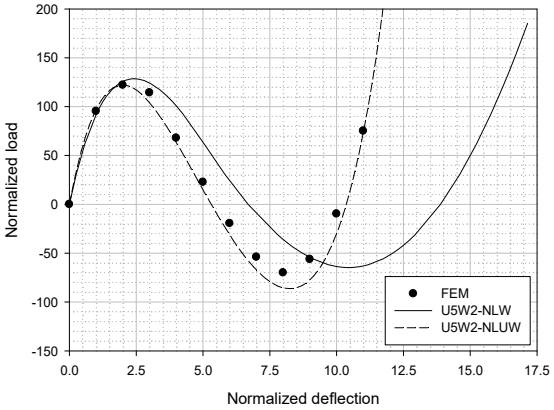

Fig. 10 Comparison of the load vs. deflection curve among U5W2-NLW, U5W2-NLUW and FEM (D_i/D_o = 0.35, h/D_o = 0.2, h/t=5.3, t/L=0.0989, β=31.61°)

The comparison with the results obtained from FEM in the Fig. 8 and 9 shows very good agreements. This confirms accuracy and reliability of the developed energy method to perform stress analysis in the spring with much fewer degrees of freedom and less computational cost than those of a FEM analysis. More details for stress and strain analysis of the Belleville spring are given in Table 2. The springs with D_i/D_o equal to 0.35, h/t equal to 1.5 and 3.3, and h/D_o equal to 0.01 and 0.05 are considered. The stress and strain in the circumferential and radial directions are computed from the energy method when the applied load is about 20% of the upper critical load. The maximum circumferential stress is compressive stress on the top surface at the inner diameter whereas the maximum radial stress is also compressive on the top surface, but at approximately the middle of the generator line due to the maximum radial curvature occurring at that point.

The strain in both directions, nonetheless, is always maximum at the inner diameter. Note that the Almen and Laszlo's assumption of zero radial stress is clearly invalid because the ratio of maximum radial stress to maximum radial circumferential stress is more than 10%, which is truly not negligible. The similar conclusion can also be made from strain analysis. The ratio of maximum radial strain to maximum circumferential strain is almost 20% and the radial strain is also not that trivial when compared to the circumferential strain. This result then refutes the zero radial strain hypothesis that is proposed by Curti and Orlando [12, 13].

3.3 Very large deflections

The preceding figures show the necessity of including the geometrically nonlinear terms of w from von Karman approximation in order to capture the nonlinear behavior of the Belleville spring. Without such terms, the relation between load and deflection is linear and the spring rate is always predicted to be constant. The energy equation that excludes the nonlinear terms can predict the characteristic of the spring only with very low deflection (δ_{nor} less than 0.25). However, a significant increment of deflection can induce stronger effect of geometrical nonlinearities. In such cases of very large deflections, Reissner's approximation expressed as the double underlined nonlinear term of u in the radial strains in Equation (16) becomes essential for accurate prediction by the energy method.

$$\varepsilon_s^o = \frac{\partial u}{\partial s} + \underline{\frac{1}{2}\left(\frac{\partial w}{\partial s}\right)^2} + \underline{\underline{\frac{1}{2}\left(\frac{\partial u}{\partial s}\right)^2}} \qquad (16)$$

Fig. 10 distinguishes spring deformations under the applied load including and not including Reissner's approximation. The spring characteristic computed from the energy method with the double underlined strain component is denoted by U5W2-NLUW legend, whereas that with merely the underlined strain component is designated by U5W2-NLW legend as consistently used in this article. The calculation from the energy method is compared with the FEM and the result obtained from U5W2-NLUW model is very close

to the finite element simulation. This indicates that the exclusion of the nonlinear term of u can overpredict the deformation when the spring deflection becomes very large. It should be noted that even though U5W2-NLUW model provides good predictions in a wider range of spring geometries and deformations, the model is quite computationally expensive because of strong nonlinearities. Thus, Reissner's approximation should be used only when the spring has h/t greater than three and is loaded so that δ_{nor} is greater than 0.25.

4. Conclusion

An application of the Ritz method based on the energy approach has been discussed to predict the deformation and load characteristics of a Belleville spring made of isotropic materials. Because of nonlinear spring rate involved, geometric nonlinearities are included in the theory and, as such, multiple spring deflections can be predicted at the same load when the spring's geometric ratios h/t and h/D_o are higher than their critical values. The snap-through action can be observed by the present energy method, as can also be seen by the seminal Almen and Laszlo formulation, but the former is shown to be more accurate and versatile than the latter when compared to the experiments and finite-element analysis in various cases.

In summary, it appears that the energy method presented herein has the enormous potential and can be further applied to predict and design a variety of novel disk springs, for example springs with non-constant thickness in order to achieve the optimal spring configurations for minimum developed stress or lowest weight with the same spring rate. This type of spring in practice has more complicated shape so it is more involved in analysis and design with the conventional models. Springs composed of a smart material such as shape memory alloy and piezoelectric materials are another example that is suited for the energy method due to the materials' sophisticated constitutive models. There are a number of promising features of smart Belleville springs that have not been investigated or studied before and they can be explored for their increasing potentials in the future.

5. Acknowledgement

The work reported on this article was accomplished while the first author was financially supported by the scholarship from Thailand Research Fund (TRF) through the Royal Golden Jubilee Ph.D. Program (Grant No. PHD/0143/2551), Shell Centennial Education Fund, Shell Companies in Thailand and graduate research scholar from KMUTT. All the grants are gratefully acknowledged.

6. References

[1] Almen, J.O. and Laszlo, A. (1936). The uniform-section disk spring, *Transaction of the ASME*, Vol. 58, 1936, pp. 305-314.

[2] Pflüger, A. (1937). Stabilität dünner Kegelschalen, *Ing. Archiv*, Vol. 8, No. 3, pp. 151–172.

[3] Seide, P. (1956). Axisymmetric buckling of circular cones under axial compression, *J Appl Mech*, Vol. 23, pp. 625-628.

[4] Seide, P. (1961). "Buckling of circular cones under axial compression," J Appl Mech, Vo. 28, 1961, pp. 315-326.

[5] Weigarten, V. I., Morgan, E. J. and Seide, P. (1965). Elastic stability of thin walled cylindrical and conical shells under axial compression, *AIAA J*, Vol. 3, pp. 500-505.

[6] Weigarten, V. I. and Seide, P. (1965). Elastic stability of thin walled cylindrical and conical shells under combined external pressure and axial compression, *AIAA J*, Vol. 3, pp. 913-920.

[7] Singer, J. (1961). Buckling of circular conical shells under axisymmetrical external pressure," *J Mech Eng Sci*, Vol. 3, pp. 330-339.

[8] Baruch, M. and Singer, J. (1965). General instability of stiffened conical shells under hydrostatic pressure, *Aero Q*, Vol. 26, pp. 187-204.

[9] Baruch, M., Harari, O. and Singer, J. (1967). Influence of in-plane boundary conditions on the stability of conical shells under hydrostatic pressure, *Israel J Technol*, Vol. 5, pp. 512-24.

[10] Baruch, M., Harari, O. and Singer, J. (1970). Low buckling loads of axially compressed conical shells, *J Appl Mech*, Vol. 37, pp. 384-392.

[11] Timoshenko, S. (1934). Strength of materials, D. Van Nostraad Company, New York, 2nd Ed.

[12] Curti, G. and Orlando, M. (1979). New Calculation Method for Disc Springs, *Wire*, Vol. 30, pp. 17-22.

[13] Curti, G. and Orlando, M. (1980). Experimental Investigation with a New Design Calculation for Disc Springs, *Wire*, Vol. 31, pp. 26-29.

[14] Zheng, E., Jia F. and Zhou, X. (2014). Energy-Based Method for Nonlinear Characteristics Analysis of Belleville springs, *J. Thin-Walled Structures*, Vol. 79, pp. 52-61.

[15] Ozaki, S. and Tsuda. K. (2012). Analyses of Static and Dynamic Behavior of Coned Disk Spring: Effects of Friction Boundaries. *J. Thin-Walled Structure*, Vol. 59, pp. 132–43.

[16] Bouzid, A. and Nechache, A. (2010). The Modelling of Bolted Flange Joints used with Disc Springs and Tube and Tube Spacers to Reduce Relaxation. *Int. J. Pressure Vessels Piping*. Vol. 87, pp. 730–6.

[17] Atxaga, G. and Pelayo, A. (2006). Failure Analysis of a Set of Stainless Steel Disc Spring. *Eng. Failure Analysis*, Vol. 16, pp. 226–34.

[18] Hyer, M. W. (2009). Stress Analysis of Fiber-Reinforced Composite Materials, DEStech Publications, Inc., Lancaster, PA USA.